



Cite this: *Phys. Chem. Chem. Phys.*,  
2019, 21, 14270

# Fast beam photofragment translational spectroscopy of the phenoxy radical at 225 nm, 290 nm, and 533 nm†

Erin N. Sullivan,<sup>ab</sup> Bethan Nichols<sup>‡ab</sup> and Daniel M. Neumark<sup>id \*ab</sup>

Photodissociation of the phenoxy radical ( $C_6H_5O$ ) is investigated using fast beam photofragment translational spectroscopy. Phenoxy radicals are generated through photodetachment of phenoxide anions ( $C_6H_5O^-$ ) at 532 nm. Following photoexcitation of the radicals at 225 nm (5.51 eV), 290 nm (4.27 eV), or 533 nm (2.33 eV), photofragments are collected in coincidence to determine their masses, translational energy, and scattering angle for each dissociation event. Two-body dissociation yields exclusively  $CO + C_5H_5$ , and three-body dissociation to  $CO + C_2H_2 + C_3H_3$  and  $CO + C_5H_4 + H$  is also seen at the two higher energies. The translational energy distributions for two-body dissociation suggest that dissociation occurs *via* internal conversion to the ground electronic state followed by statistical dissociation. The absorption of an additional 532 nm photon in the photodetachment region provides some  $C_6H_5O$  radicals with an additional 2.33 eV of energy, leading to much of the two-body dissociation observed at 533 nm and the three-body dissociation at the two higher excitation energies.

Received 2nd November 2018,  
Accepted 11th December 2018

DOI: 10.1039/c8cp06818f

rsc.li/pccp

## 1. Introduction

The phenoxy radical ( $C_6H_5O$ ) is a significant player in the combustion chemistry of aromatic hydrocarbons<sup>1,2</sup> and participates in the redox cycle of galactose oxidase, a relevant enzyme for biological alcohol oxidation.<sup>3</sup> As such,  $C_6H_5O$  has been examined on a variety of fronts, both experimentally and theoretically, to elicit a fundamental understanding of its nature and reactivity in several different chemical arenas. The available literature of this radical is vast, ranging from spectroscopic characterization to theoretical reactivity investigations. While the secondary dissociation of  $C_6H_5O$  from anisole has provided some insight into its decomposition dynamics,<sup>4</sup> there has yet to be a direct probe into  $C_6H_5O$  photodissociation. Here, we report the photodissociation of  $C_6H_5O$  at 225 nm, 290 nm, and 533 nm using fast beam photofragment translational spectroscopy.

Electron spin resonance experiments on the phenoxy radical find that in its ground electronic state ( $\tilde{X}^2B_1$ ), electron spin

density is predominantly on the aromatic ring while the C–O bond has more double bond character.<sup>5,6</sup> Raman spectroscopy later confirmed this finding,<sup>7,8</sup> in addition to providing vibrational characterization of  $C_6H_5O$  in combination with infrared absorption spectroscopy.<sup>7–9</sup> Electronic absorption spectroscopy of  $C_6H_5O$ <sup>10,11</sup> has identified four prominent electronic excited states at 16 000 ( $\tilde{B}^2A_2$ ), 25 200 ( $\tilde{C}^2B_1$ ), 33 900 ( $\tilde{D}^2A_2$ ), and 41 800 ( $\tilde{E}^2B_1$ )  $cm^{-1}$ , each corresponding to a  $\pi \rightarrow \pi^*$  transition.<sup>12</sup> The optically forbidden  $n \rightarrow \pi^*$ ,  $\tilde{A}^2B_2 \leftarrow \tilde{X}^2B_1$  transition has been characterized using cavity ring-down absorption spectroscopy yielding the assignment of eight vibronic bands and a weak origin feature at 7681  $cm^{-1}$ .<sup>12,13</sup> The electron affinity of  $C_6H_5O$  was first determined through anion photodetachment<sup>14,15</sup> and a refined value of 2.2538(8) eV was subsequently measured *via* slow electron velocity map imaging.<sup>16,17</sup>

In regards to unimolecular dissociation, the  $C_6H_5O$  radical has been identified as a product of phenol and anisole photodissociation.<sup>4,18–20</sup> Infrared multiphoton dissociation of anisole yields  $C_6H_5O$ , which further fragments into  $CO + C_5H_5$  with a translational energy distribution peaking around 0.6 eV and extending to 2.0 eV.<sup>4</sup> This large translational energy release was attributed to a high exit barrier on the ground electronic state. H atom loss from phenol also results in  $C_6H_5O$  production with very little vibrational energy imparted to the radical.<sup>18,19</sup> Additionally, thiophenoxy ( $C_6H_5S$ ), a relevant analog to  $C_6H_5O$ , has been studied using fast beam photofragment translational spectroscopy at multiple wavelengths<sup>21</sup> with the major products being  $CS + C_5H_5$  and  $SH + C_6H_4$ . That study

<sup>a</sup> Department of Chemistry, University of California, Berkeley, California 94720, USA. E-mail: dneumark@berkeley.edu

<sup>b</sup> Chemical Sciences Division, Lawrence Berkeley National Laboratory, Berkeley, California 94720, USA

† Electronic supplementary information (ESI) available: Photoelectron assignments, 193 nm dissociation data, and results of RRM calculations. See DOI: 10.1039/c8cp06818f

‡ Present address: Thumbtack, San Francisco, CA 94103, USA.

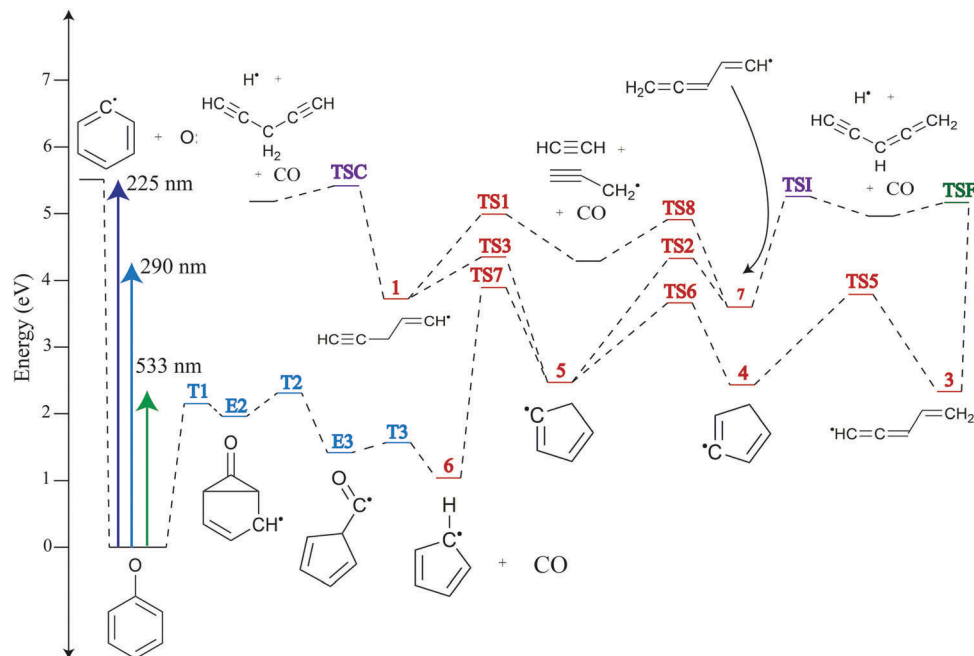
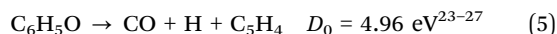
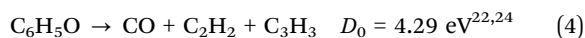
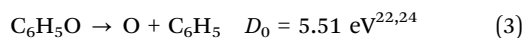
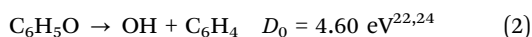


Fig. 1 Potential energy surface of  $C_6H_5O$  dissociation. Different colors indicate the references from which geometries, stationary points, and vibrational frequencies were taken for theoretical calculations. Energies of the blue, red, purple, and green points were taken from ref. 32, 27, 26, and 33, respectively, and corresponding notations are consistent with those used in each source. Product channel energies are shown in black and were determined *via* experimental heats of formation.

concluded that the products are formed by internal conversion followed by dissociation on the ground electronic state.

Possible dissociation channels of  $C_6H_5O$  are listed in eqn (1)–(5):



Several theoretical studies have examined the mechanism by which  $C_6H_5O$  decays to  $CO + C_5H_5$ .<sup>28–31</sup> Fig. 1 presents a potential energy surface depicting CO loss<sup>32</sup> and secondary dissociation of  $C_5H_5$ , which is energetically possible at some wavelengths used here and can either result in H atom loss or decomposition to acetylene ( $C_2H_2$ ) + propargyl radical ( $C_3H_3$ ).<sup>33</sup> The lowest energy pathway to dissociation involves the formation of the bicyclic species (E2) that then undergoes ring-opening to a five-membered ring and subsequent bond cleavage to lose CO.  $C_6H_5O$  can also lose O or OH fragments through simple bond cleavage, but these channels are considerably higher in energy and require an additional 4 eV of energy at least.

We report the results of the photodissociation of  $C_6H_5O$  at 225 nm (5.51 eV), 290 nm (4.27 eV), and 533 nm (2.33 eV) using fast beam photofragment translational spectroscopy. These wavelengths correspond to excitation of the  $\tilde{E}^2B_1$ ,  $\tilde{D}^2A_2$ , and  $\tilde{B}^2A_2$  electronic states, respectively. At all three wavelengths,

the sole two-body channel is  $CO + C_5H_5$  (channel 1). The associated translational energy and angular distributions are markedly similar for each dissociation wavelength, suggesting statistical dissociation on the ground electronic state and matching previous inferences from the secondary dissociation of  $C_6H_5O$  from anisole.<sup>4</sup> Energetic constraints and theoretical calculations suggest that channel 1 from excitation at 533 nm mostly occurs when the original  $C_6H_5O$  radical absorbs an auxiliary photon of 532 nm in the photodetachment region of the instrument prior to interacting with the dissociation laser beam. The three-body channels 4 ( $CO + C_2H_2 + C_3H_3$ ) and 5 ( $CO + H + C_5H_4$ ) are observed at 225 nm and 290 nm. These channels are also attributed to  $C_6H_5O$  radicals that have absorbed a 532 nm photon prior to UV excitation.

## II. Methods

### A. Experimental

The fast radical beam machine has been outlined previously.<sup>34,35</sup> In brief, phenoxide anions ( $C_6H_5O^-$ ) were produced by bubbling 20 psig of  $N_2O/Ar$  through benzene (Fisher Scientific). The resulting gas mixture was introduced into vacuum through an Amsterdam Piezovalve<sup>36,37</sup> and then passed through a DC discharge<sup>38</sup> stabilized by an electron gun. The ions were accelerated to high kinetic energies (6–8 keV), mass-selected using a Bakker time-of-flight mass spectrometer,<sup>39,40</sup> and steered to the detachment region where the 532 nm output of an Nd:YAG laser (Litron LPY 742-100) was used to remove an electron from  $C_6H_5O^-$ , yielding a fast beam of neutral phenoxy ( $C_6H_5O$ ) radicals.

A photoelectron spectrometer used to characterize the radicals sits perpendicular to the beam path such that detached electrons are extracted using velocity-map imaging and detected *via* chevron mounted microchannel plates coupled to a phosphor screen and CCD camera (Beam Imaging Solutions BOS-75).<sup>35</sup> Analysis of the acquired images was carried out using the Inverse Abel Transformation (BASEX).<sup>41</sup>

Following electron detachment, any remaining  $C_6H_5O^-$  anions left in the beam were deflected and the neutral radicals were dissociated. Excitation wavelengths of 225 nm (5.51 eV), 290 nm (4.27 eV) and 533 nm (2.33 eV) were generated using an XeCl excimer-pumped dye laser (Lambda Physik LPX 200 and FL 3002), of which the doubled output was used to produce 225 nm and 290 nm. Fragments from two and three-body dissociation processes were acquired in coincidence by a Roentdek Hex80 delay-line detector<sup>21,42</sup> to yield the fragment masses, translational energy release, and scattering angle for each dissociation event. The overall distributions of these quantities were obtained from data sets that typically comprised 5000 to 15 000 valid coincident events obtained over 6–8 hours. A beam block, 2.5 mm in diameter, which sits  $\sim 49$  cm in front of the detector, prevented undissociated radicals from impinging upon the detector. Due to the presence of this beam block and the finite size of the detector, translational energy distributions presented here have been corrected by a detector acceptance function (DAF).<sup>34</sup>

We observed the acquisition of coincident events in instances during which the photodetachment laser was on but the dissociation laser off. This was evidence for the dissociation of  $C_6H_5O$  from additional 532 nm photons absorbed in the photodetachment region. Using the molar extinction coefficient from Radziszewski *et al.*,<sup>12</sup> we estimate the fraction of absorption to occur for about  $\sim 3\%$  of  $C_6H_5O$  still in the photodetachment region. The role of this absorption is considered in Sections III and IV.

## B. Theoretical

To aid in understanding the dissociation results, the Rice–Ramsperger–Kassel–Marcus (RRKM) approximation was employed to predict the rate constants for statistical dissociation processes, specifically that of the primary dissociation  $C_6H_5O$  and the secondary dissociation of  $C_5H_5$ .<sup>43</sup> The RRKM microcanonical rate constant is given by:

$$k(E) = \frac{W^\ddagger(E - E_0)}{h\rho(E)} \quad (6)$$

where  $W^\ddagger(E - E_0)$  is the sum of states of the transition state,  $\rho(E)$  is the density of states of the reactant, and  $h$  is Planck's constant. The vibrational density and sum of states were calculated using the Beyer–Swinehart algorithm,<sup>44</sup> and the steady state approximation was used for intermediate structures. Geometries for  $C_6H_5O$  and relevant intermediate and transition state species leading to dissociation were acquired from Olivella *et al.*<sup>30</sup> and reoptimized at the B3LYP/6-311+G(d,p) level of theory. Energies of stationary points were calculated at G3X-K level of theory from ref. 32. In their work on  $C_5H_5$

photodissociation, Shapero *et al.*<sup>33</sup> compiled a potential energy surface from a variety of sources<sup>25–27</sup> which was used for the calculations performed here on  $C_5H_5$  secondary dissociation. Geometries, stationary points, and vibrational frequencies were taken from the respective sources as marked in Fig. 1. The RRKM rate constants are presented in Table S2 of the ESI† for both  $C_6H_5O$  primary and  $C_5H_5$  secondary dissociation.

## III. Results

### A. Anion photoelectron spectroscopy

Fig. 2 shows the anion photoelectron spectrum of  $C_6H_5O^-$  acquired at 532 nm. This is the wavelength used to generate the radicals in the dissociation experiments, so the photoelectron spectrum reflects the vibrational distribution of the radicals formed by photodetachment.

The black trace corresponds to the experimental spectrum while the red corresponds to Franck–Condon simulations.  $C_6H_5O^-$  and  $C_6H_5O$  geometries and frequencies were determined *via* DFT using the B3LYP/6-311+g(d,p) level of theory in the Gaussian 09 package.<sup>45</sup> Frequencies were scaled by 0.9679 in accordance with the rules appropriate for Pople style basis sets.<sup>46</sup> Franck–Condon simulations were then carried out using ezSpectrum<sup>47</sup> at an assumed vibrational temperature of 300 K. As can be seen from Fig. 2, the experiment and simulations match reasonably well. Table S1 in the ESI† presents the specific peak assignments, but in brief, peak B corresponds to the vibrational origin. From this, the electron affinity is determined to be  $2.253 \pm 0.001$  eV which is good agreement with the previous reported value of 2.2538(8) eV.<sup>16</sup>

In addition to the origin, the most intense feature is labeled D and is attributed to the addition of one quantum of energy into the  $\nu_{11}$  in-plane CCC bend, while peaks A and C correspond to transitions from anions excited in the  $\nu_{14}$  mode that corresponds to a ring deformation out-of-plane rocking of opposite carbon atoms. These assignments are consistent with

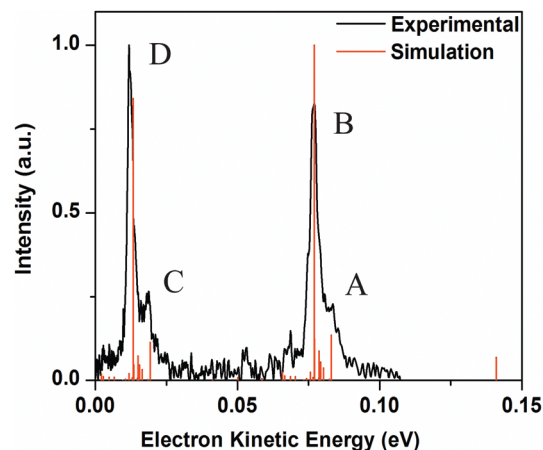


Fig. 2 Anion photoelectron spectrum of  $C_6H_5O^-$  taken at 532 nm. The black trace shows the experimental spectrum while the red presents the Franck–Condon simulations. The peaks are labelled and tabulated in Table S1 in the ESI.†

those previously reported by Kim *et al.*,<sup>16</sup> thereby confirming the formation of the  $C_6H_5O$  radical in our experiment.

One purpose of acquiring photoelectron spectra in our experiment is to characterize the internal energy of the radicals produced by photodetachment, referred to as  $E_{INT,R}$ . This internal energy can arise from vibrational excitation of the anions that is retained upon photodetachment, as well as excitation of the neutrals resulting from photodetachment at photon energies above the vibrational origin. While feature A corresponds to a hot band, this amount of energy is  $<0.10$  eV and feature B (the vibrational origin) is significantly more intense than feature A, implying that many  $C_6H_5O$  radicals are produced in their ground vibrational state. Feature D, which corresponds to one quantum of excitation in the  $\nu_{11}$  mode, is slightly more intense than feature B but is only  $\sim 0.06$  eV above the vibrational origin. Therefore, in moving forward, we approximate  $E_{INT,R}$  as 0 eV.

### B. Photofragment mass distributions

The two and three-body mass distributions from  $C_6H_5O$  dissociation at excitation wavelengths of 225 nm, 290 nm, and 533 nm are presented in Fig. 3 in blue, red, and green, respectively. In the two-body distribution (Fig. 3a), there are two narrow peaks at 28 and 65 Da for all three dissociation wavelengths, and these masses are consistent with the formation of channel 1 ( $CO + C_5H_5$ ). Fig. 3b presents the three-body mass distributions. For one photon at 533 nm (2.33 eV), there are no energetically accessible three-body channels and none are observed. At 225 nm and 290 nm, three-body dissociation is observed despite the fact that at 290 nm, the possible three-body channels are not energetically attainable, which suggests excess energy within the system. The distributions for 225 nm and 290 nm each include one large feature spanning 26–28 Da and a second smaller feature around 39 Da. These peaks are primarily attributed to channel 4 ( $CO + C_2H_2 + C_3H_3$ ); we do not expect to resolve CO and  $C_2H_2$ , and the peak at lower mass is slightly more than twice ( $\sim 2.3$  times) as intense as that at 39 Da.

In addition to the larger features corresponding to channel 4, there are also smaller peaks close to 1 and 64 Da that correspond to H atom +  $C_5H_4$  production, respectively, *i.e.* two of the three fragments from channel 5 ( $CO + H + C_5H_4$ ). The third fragment, CO, presumably accounts for the additional intensity (*i.e.* beyond a factor of two) in the large feature at 28 Da that is not from channel 4.

### C. Translational energy distributions

For single-photon excitation, the translational energy  $E_T$  imparted to dissociating fragments is related to the photon energy  $h\nu$ , the product channel dissociation energy  $D_0$ , the internal energy of the initial radical  $E_{INT,R}$ , and the internal energy of the products  $E_{INT,P}$ , through the following expression:

$$E_T = h\nu - D_0 + E_{INT,R} - E_{INT,P} \quad (7)$$

As was already discussed in Section III A,  $E_{INT,R}$  is taken to be 0 eV. Fig. 4 presents the translational energy distribution for

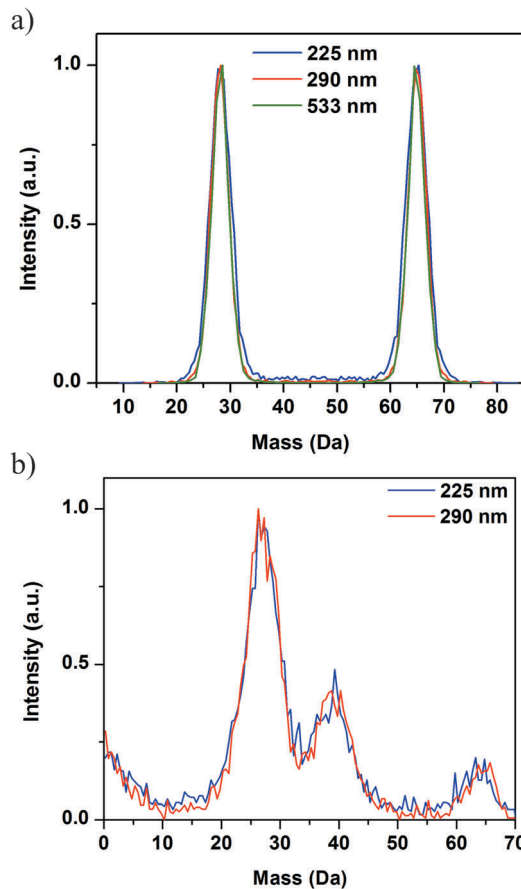


Fig. 3 Photofragment mass distributions of  $C_6H_5O$  dissociation. Panel a presents the two-body distribution for experiments performed at 225 nm (blue), 290 nm (red), and 533 nm (green). Panel b presents the three-body distributions at 225 nm (blue) and 290 nm (red).

$C_6H_5O$  dissociation to channel 1 ( $CO + C_5H_5$ ) from excitation at 225 nm (blue), 290 nm (red), and 533 nm (green). The distributions are very similar at each dissociation wavelength, peaking just below 1.0 eV and extending to 2.0 eV.  $E_{T,MAX}$  for this

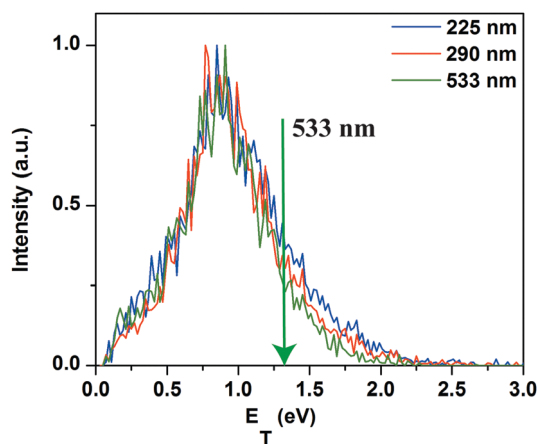


Fig. 4 Two-body translational energy distribution of  $C_6H_5O$  to channel 1 ( $CO + C_5H_5$ ) at 225 nm (blue), 290 nm (red), and 533 nm (green). The green arrow marks  $E_{T,MAX}$  for dissociation at 533 nm.

channel is 4.51 eV (225 nm), 3.23 eV (290 nm), and 1.29 eV (533 nm), the former two of which are not marked as they are beyond the scale of the  $x$ -axis. The associated angular distributions for all dissociation wavelengths are isotropic.

It is clear from Fig. 1 that the production of CO + C<sub>5</sub>H<sub>5</sub> through channel 1 requires traversing barriers that are comparable to 533 nm (2.33 eV), so it is unlikely that excitation by a single 533 nm photon would lead to dissociation. Additionally, the green trace extends  $\sim 0.7$  eV beyond  $E_{T,MAX}$  for 533 nm, thereby suggesting that some additional energy is provided to C<sub>6</sub>H<sub>5</sub>O to result in dissociation at this wavelength. This additional energy is attributed to a two-photon process in the photodetachment region: photodetachment of C<sub>6</sub>H<sub>5</sub>O<sup>-</sup> at 532 nm followed by absorption of a 532 nm photon by C<sub>6</sub>H<sub>5</sub>O. The implications of this mechanism are discussed further in Section IV.

Fig. 5 presents the translational energy distribution for dissociation of channel 4 (CO + C<sub>2</sub>H<sub>2</sub> + C<sub>3</sub>H<sub>3</sub>) at 225 nm (blue) and 290 nm (red) in panel a. For a single photon at 290 nm, this channel is not energetically accessible, which is again indicative of excess energy in the system. At 225 nm, channel 4 is energetically accessible, but as can be seen in Fig. 5, the distribution extends beyond  $E_{T,MAX}$  for a single photon at this wavelength. In Fig. 5a,  $E_{T,MAX}$  for 532 nm + 290 nm (6.60 eV) is marked by the red arrow, while the two blue arrows mark  $E_{T,MAX}$  for 225 nm (5.51 eV) and 532 nm + 225 nm (7.84 eV), respectively. Since the translational energy distributions extend beyond  $E_{T,MAX}$  for a single photon at 290 nm or 225 nm, it appears that much, if not all, of channel 4 results from photodissociation of radicals that have already absorbed a 532 nm photon in the photodetachment region *via* the process described in the preceding paragraph. The two distributions show the same rising edge, peaking around 1.0 eV, but the blue trace extends to higher energies.

Panels b and c in Fig. 5 present Dalitz plots for C<sub>6</sub>H<sub>5</sub>O dissociation to channel 4 at 225 nm (b) and 290 nm (c). Dalitz plots

are a tool for understanding the translational energy partitioning amongst the three fragments, in which  $\epsilon_i$  refers to the fraction of translational energy imparted to fragment  $i$  where  $0 \leq \epsilon_i \leq 1$ .<sup>48</sup> Conservation of energy restricts all events to lie within the triangle, while conservation of momentum requires all events to lie within the ellipse. By examining a Dalitz plot, we can obtain an understanding for how the three-body dissociation event proceeds. While the plots in Fig. 5b and c appear relatively uniform, there is a light band of intensity in upper left region of the ellipse in Fig. 5b highlighted between the dashed orange lines. This feature also appears in Fig. 5c but is less distinguishable. The associated angular distributions for channel 4 are isotropic at both wavelengths.

Fig. 6 presents the translational energy distributions for dissociation of C<sub>6</sub>H<sub>5</sub>O to channel 5 (CO + H + C<sub>5</sub>H<sub>4</sub>). The distributions for both dissociation wavelengths peak just beyond 1.0 eV and tail off near  $E_{T,MAX}$  for 532 nm + 290 nm, indicating that this channel also arises from radicals that have absorbed a 532 nm photon in the photodetachment region. The Dalitz plots for this channel are not shown as they do not present a holistic representation of the data due to low event count. The associated angular distributions are isotropic.

## IV. Discussion

### A. Two-body dissociation

Channel 1 (CO + C<sub>5</sub>H<sub>5</sub>) is the only observed two-body dissociation pathway of C<sub>6</sub>H<sub>5</sub>O. The translation energy distributions are markedly similar for each dissociation wavelength and the associated angular distributions are isotropic. These distributions point to a dissociation mechanism in which the C<sub>6</sub>H<sub>5</sub>O internally converts to its ground electronic state and then dissociates statistically. Studies examining the electronic absorption spectrum of C<sub>6</sub>H<sub>5</sub>O<sup>12,49</sup> have shown that 225 nm, 290 nm, and 533 nm correspond to excitation of the  $\tilde{E}^2B_1$ ,

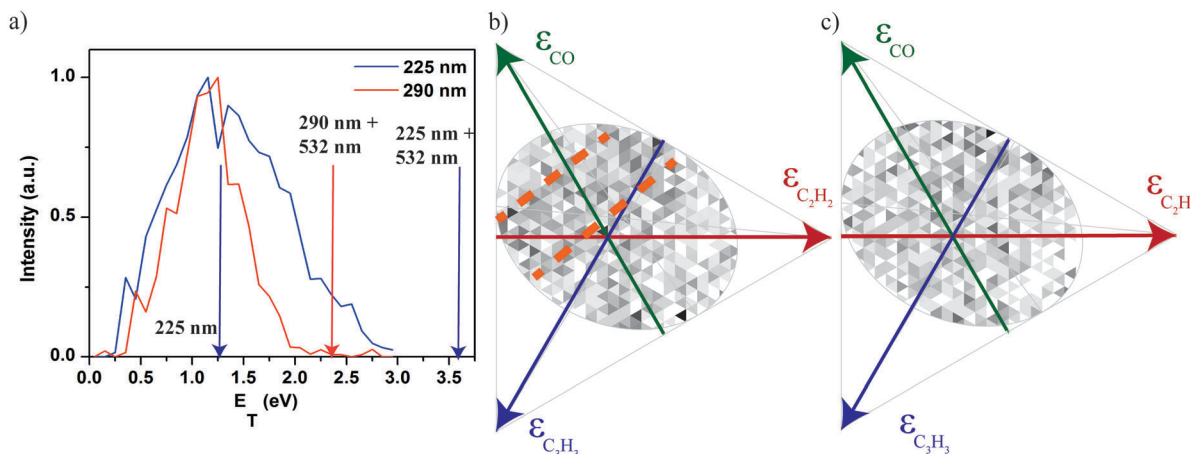


Fig. 5 (a) Three-body translational energy distribution of C<sub>6</sub>H<sub>5</sub>O to channel 4 (CO + C<sub>2</sub>H<sub>2</sub> + C<sub>3</sub>H<sub>3</sub>) at 225 nm (blue) and 290 nm (red). The arrows mark  $E_{T,MAX}$  in corresponding colors. A single photon of 290 nm is insufficient in energy to produce channel 4, but with the absorption of a 532 nm photon, channel 4 is accessible. Therefore,  $E_{T,MAX}$  for the absorption of an additional 532 nm photon is marked as well. Dalitz plots of three-body dissociation of C<sub>6</sub>H<sub>5</sub>O to channel 4 at 225 nm and 290 nm are shown in panels b and c, respectively.

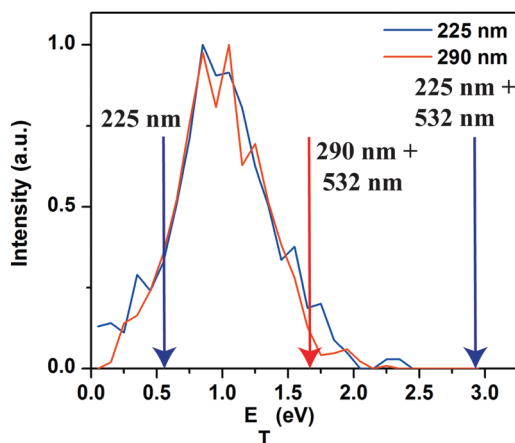


Fig. 6 Three-body translational energy distribution of  $C_6H_5O$  to channel 5 ( $CO + H + C_5H_4$ ) at 225 nm (blue) and 290 nm (red). The arrows mark  $E_{T,MAX}$  in corresponding colors. A single photon of 290 nm is insufficient in energy to produce channel 5 and a photon of 225 nm only just possesses enough energy. Absorption of a 532 nm photon in the detachment region, followed by absorption of 225 nm or 290 nm can also lead to channel 5 production. Therefore,  $E_{T,MAX}$  referring to the maximum available energy for these combination of energies is also marked in corresponding colored arrows.

$\tilde{D}^2A_2$ , and  $\tilde{B}^2A_2$  electronic states, respectively. For repulsive dissociation on an excited state surface, an alternate mechanism, the excitation to three distinct electronic states would likely yield markedly different translational energy distributions, and this is not seen here.

The ground state mechanism is supported by comparison to the work carried out by Schmoltner *et al.*<sup>4</sup> in which infrared multiphoton dissociation (IRMPD) of anisole was studied and the secondary dissociation of the  $C_6H_5O$  product generated  $CO + C_5H_5$ ; these processes are governed by statistical ground state dynamics. The corresponding translational release of the secondary products peaked around 0.6 eV and extended to 2.0 eV, similar to the distributions seen here. Theoretical work examining the secondary dissociation of anisole attributed the large translational release to a substantial barrier<sup>29</sup> of 44 kcal mol<sup>-1</sup> to produce  $CO + C_5H_5$  but did not discuss the actual mechanism or intermediates leading to dissociation.<sup>4</sup> The somewhat more recent work by Olivella *et al.*<sup>30</sup> and Hemberger *et al.*<sup>32</sup> (presented in blue in Fig. 1) shows that there are several intermediate processes to dissociation: cyclization is followed by the rate limiting step in which the cyclopropanone ring is opened with a barrier of about 2.6 eV to form the (2,4-cyclopentadienyl)carbonyl radical succeeded by a slight barrier to CO loss.<sup>30</sup> With such high energies to traverse prior to dissociation, the large translational energy release seen in our work and the IRMPD study is not surprising.

Statistical dissociation on the ground electronic state is also consistent with the work done by Harrison *et al.*<sup>21</sup> in which  $C_6H_5S$ , a comparable system, was observed to dissociate into  $CS + C_5H_5$  and  $SH + C_6H_4$ . The observed dissociation to  $CS + C_5H_5$  was attributed to ground state dissociation; the pathway involving rearrangement to get these products is identical to

that which would occur to produce channel 1 from  $C_6H_5O$ , although the asymptotic energetics are quite different owing to the high stability of CO.

As was mentioned in Section III C, the translational energy distribution for formation of channel 1 from 533 nm extends beyond  $E_{T,MAX}$ , and the energy of one 533 nm photon (2.33 eV) is barely above the energy required to traverse TS2 (Fig. 1). These observations suggest a source of excess energy contributing to the dissociation of  $C_6H_5O$  at this wavelength. They can be explained by our observation of coincident events when the dissociation laser was off, suggesting that some  $C_6H_5O$  radicals, upon formation through photodetachment, absorb an additional 532 nm (2.33 eV) photon while still in the vicinity of the photodetachment laser beam but do not dissociate prior to their interaction with the second laser pulse. The RRKM dissociation rate constant for a  $C_6H_5O$  radical that absorbs one photon of 532 nm and internally converts to the ground state is on the order of 1 s<sup>-1</sup> (Table S2, ESI<sup>†</sup>), which suggests that such a radical survives during its transit to the dissociation region ( $\sim 5$   $\mu$ s travel time) where it can then absorb a second photon. Therefore, the majority of dissociation to channel 1 at 533 nm is attributed to a two-photon process in which  $C_6H_5O$  absorbs a 532 nm photon in the photodetachment region and a second photon of 533 nm in the photodissociation region.

As discussed in Section III B, those radicals that absorb a 532 nm photon and are then excited at 290 nm or 225 nm undergo three-body dissociation. At these excitation energies, prior absorption of a 532 nm photon provides an additional 2.33 eV of energy to the system (7.84 eV and 6.60 eV for 532 nm + 225 nm and 532 nm + 290 nm, respectively) such that  $C_5H_5$  can be imparted with sufficient internal energy to dissociate further. Hence, at 225 nm and 290 nm the two-body dissociation yielding channel 1 is attributed exclusively to one photon excitation, *i.e.* it originates from  $C_6H_5O$  radicals that have not absorbed an additional photon of 532 nm.

## B. Three-body dissociation

$C_6H_5O$  three-body dissociation leads to the production of channels 4 ( $CO + C_2H_2 + C_3H_3$ ) and 5 ( $CO + H + C_5H_4$ ), both of which are observed at 290 nm and 225 nm. At 290 nm, channels 4 and 5 are not energetically possible, suggesting that both channels must stem from a two-photon process at this wavelength. At 225 nm, both channels are allowed, so a more thorough analysis is required to determine the role of a one- versus two-photon process and the mechanism to three-body production. Based on the potential energy surface in Fig. 1 and the established ground state mechanism for two-body dissociation, a reasonable scenario for three-body dissociation from either a one- or two-photon process is internal conversion to the ground state, loss of CO, and then dissociation of the  $C_5H_5$  fragment if it is left with sufficient internal energy.

With this mechanism in mind, RRKM calculations, the results of which are shown in Table S2 (ESI<sup>†</sup>), provide considerable insight into the three-body dissociation dynamics. At 225 nm, the RRKM calculations predict dissociation rate constants of  $C_5H_5$  to channels 4 and 5 on the order of 10<sup>6</sup> s<sup>-1</sup>

and  $10^3 \text{ s}^{-1}$ , respectively, assuming the initial  $\text{C}_5\text{H}_5$  radical has access to all of the available energy ( $h\nu - D_0$ ) after the primary dissociation event. Channel 5 thus cannot be detected within the timescale of our experiment for one 225 nm photon, but channel 4 can be. However, when considering that much of channel 1 is produced with around 1.0 eV of translational energy and that CO likely contains some internal energy, it is unreasonable to assume that  $\text{C}_5\text{H}_5$  has access to all of the available energy ( $h\nu - D_0$ ) at 225 nm. Estimating the translational energy of channel 1 to be 1.0 eV and subtracting this from the maximum available energy to  $\text{C}_5\text{H}_5$  results in too little energy to traverse all of the barriers required to produce channel 4, without even considering the internal energy of the co-fragment CO, which would also detract from that available to  $\text{C}_5\text{H}_5$ . Hence, secondary dissociation to produce channel 4 would not likely occur for a single photon of 225 nm.

For the absorption of an additional 532 nm photon in the photodetachment region, followed by the absorption of 290 nm or 225 nm, Table S2 (ESI<sup>†</sup>) presents the RRKM rate constants which are  $10^7 \text{ s}^{-1}$  and greater for both channels, allowing for sufficient time to be detected in our experiment. These considerations imply that for  $\text{C}_6\text{H}_5\text{O}$  radicals that have absorbed 532 nm + 290 nm or 532 nm + 225 nm, primary dissociation to channel 1 is accompanied by secondary dissociation as the  $\text{C}_5\text{H}_5$  radical contains sufficient internal energy to further fragment. Therefore, in the instances in which a  $\text{C}_6\text{H}_5\text{O}$  radical absorbs an auxiliary 532 nm photon followed by 290 nm or 225 nm, channel 1 is not ultimately observed because secondary dissociation of  $\text{C}_5\text{H}_5$  yields three-body dissociation to channels 4 and 5. While we did not perform a rigorous power study of the photofragment yield as a function of 532 nm laser power, a quadratic power dependence is observed in examining the number of coincident events as a function of a few different powers of 532 nm. This is particularly true for three-body coincident events, providing further evidence of a two-photon process.

The translational energy distributions (Fig. 5a and 6) for channels 4 and 5 look similar for both dissociation wavelengths, although the blue trace in Fig. 5a extends to higher translational energies for channel 4 production at 225 nm, which may be expected given the excess energy available to photofragments. Interestingly, this is not the case for channel 5. However, the barrier height with respect to products is about 0.65 eV for channel 4 formation *versus* 0.22 eV for channel 5, as seen in Fig. 1. The higher barrier for channel 4 production allows for more energy along the reaction coordinate to manifest as translational energy. In both cases, there are multiple pathways, wells, and barriers en route to the three-body products, so predicting the effect of excitation energy on the translational energy distribution is not straightforward. Both distributions peak generally much lower than the two-photon  $E_{\text{T,MAX}}$  for each wavelength, and in combination with the associated isotropic angular distributions, provide independent support for a ground state dissociation mechanism.

The Dalitz plots in Fig. 5b and c provide additional information on channel 4. While they appear mostly uniform,

particularly in Fig. 5c where there are fewer events, Fig. 5b contains two dashed orange lines to highlight a band in the upper left portion of the plot. This region is slightly more intense than the remainder of the plot and forms a broad stripe perpendicularly intersecting the green arrow. This is indicative of a relatively constant (and generally larger) fraction of the translational energy going to CO, while the  $\text{C}_2\text{H}_2$  and  $\text{C}_3\text{H}_3$  fragments receive a varied quantity. This is consistent with fragmentation of  $\text{C}_6\text{H}_5\text{O}$  into  $\text{CO} + \text{C}_5\text{H}_5$ , followed by dissociation of  $\text{C}_5\text{H}_5$  because the partitioning of energy to the CO fragment remains consistent, while the energy fractions imparted to  $\text{C}_2\text{H}_2$  and  $\text{C}_3\text{H}_3$  are now also dependent upon the  $\text{C}_5\text{H}_5$  dissociation process.

## V. Conclusions

Photodissociation of the phenoxy radical ( $\text{C}_6\text{H}_5\text{O}$ ) has been examined at 225 nm, 290 nm, and 533 nm. Excited radicals undergo internal conversion to the ground electronic state followed by statistical dissociation to yield the primary dissociation products  $\text{CO} + \text{C}_5\text{H}_5$ . The majority of this two-body dissociation at 533 nm results from events in which  $\text{C}_6\text{H}_5\text{O}$  absorbs a 532 nm photon in the photodetachment region. At 290 nm and 225 nm, secondary dissociation of  $\text{C}_5\text{H}_5$  to yield  $\text{CO} + \text{C}_2\text{H}_2 + \text{C}_3\text{H}_3$  or  $\text{CO} + \text{H} + \text{C}_5\text{H}_4$  occurs for those radicals that have absorbed an additional photon of 532 nm prior to encountering the dissociation laser, and these channels are attributed to form on the ground electronic state in a sequential manner. These results are consistent with other experimental work examining the production and secondary dissociation of phenoxy as well as that of other analogs such as thiophenoxy.

## Conflicts of interest

There are no conflicts of interest to declare.

## Acknowledgements

The authors would also like to thank Mark Shapero and Isaac Ramphal for assistance with some theoretical work regarding  $\text{C}_5\text{H}_5$  dissociation. This research was supported by the Director, Office of Basic Energy Science, Chemical Sciences Division of the U.S. Department of Energy under Contract No. DE-AC02-05CH11231.

## References

- 1 D. S. Haynes, in *Fossil Fuel Combustion*, ed. W. Bartok and A. F. Sarofim, Wiley, New York, 1991, p. 261.
- 2 H. Bockhorn, *Soot Formation in Combustion*, Springer-Verlag, New York, 1995.
- 3 S. Itoh, M. Taki and S. Fukuzumi, *Coord. Chem. Rev.*, 2000, **198**, 3–20.
- 4 A.-M. Schmoltner, D. S. Anex and Y. T. Lee, *J. Phys. Chem.*, 1992, **96**, 1236–1240.

- 5 W. T. Dixon and R. O. C. Norman, *J. Chem. Soc.*, 1964, 4857–4860.
- 6 W. T. Dixon and D. Murphy, *J. Chem. Soc., Faraday Trans. 2*, 1976, 1221–1230.
- 7 G. N. R. Tripathi and R. H. Schuler, *J. Chem. Phys.*, 1984, **81**, 113–121.
- 8 A. Mukherjee, M. L. McGlashen and T. G. Spiro, *J. Phys. Chem.*, 1995, **99**, 4912–4917.
- 9 J. Spanget-Larsen, M. Gil, A. Gorski, D. M. Blake, J. Waluk and J. G. Radziszewski, *J. Am. Chem. Soc.*, 2001, **123**, 11253–11261.
- 10 G. Porter and F. J. Wright, *Trans. Faraday Soc.*, 1955, **51**, 1469–1474.
- 11 K. Tonokura, T. Ogura and M. Koshi, *J. Phys. Chem. A*, 2004, **108**, 7801–7805.
- 12 J. G. Radziszewski, M. Gil, A. Gorski, J. Spanget-Larsen, J. Waluk and B. J. Mróz, *J. Chem. Phys.*, 2001, **115**, 9733–9738.
- 13 C.-W. Cheng, H. Witek and Y.-P. Lee, *J. Chem. Phys.*, 2008, **129**, 154307.
- 14 J. H. Richardson, L. M. Stephenson and J. I. Brauman, *J. Am. Chem. Soc.*, 1975, **97**, 2967–2970.
- 15 R. F. Gunion, M. K. Gilles, M. L. Polak and W. C. Lineberger, *Int. J. Mass Spectrom. Ion Processes*, 1992, **117**, 601–620.
- 16 J. B. Kim, T. I. Yacovitch, C. Hock and D. M. Neumark, *Phys. Chem. Chem. Phys.*, 2011, **13**, 17378–17383.
- 17 S. J. Kregel and E. Garand, *J. Chem. Phys.*, 2018, **149**, 074309.
- 18 M. G. D. Nix, A. L. Devine, B. Cronin, R. N. Dixon and M. N. R. Ashfold, *J. Chem. Phys.*, 2006, **125**, 133318.
- 19 M. N. R. Ashfold, B. Cronin, A. L. Devine, R. N. Dixon and M. G. D. Nix, *Science*, 2006, **312**, 1637–1640.
- 20 C.-M. Tseng, Y. T. Lee, M.-F. Lin, C.-K. Ni, S.-Y. Liu, Y.-P. Lee, Z. F. Xu and M. C. Lin, *J. Phys. Chem. A*, 2007, **111**, 9463–9470.
- 21 A. W. Harrison, J. S. Lim, M. Ryazanov, G. Wang, S. Gao and D. M. Neumark, *J. Phys. Chem. A*, 2013, **117**, 11970–11978.
- 22 W. Tsang, in *Energetics of Organic Free Radicals*, ed. J. A. M. Simoes, A. Greenberg and J. F. Liebman, Blackie Academic and Professional, London, 1996, pp. 22–58.
- 23 T. L. Nguyen, T. N. Le and A. M. Mebel, *J. Phys. Org. Chem.*, 2001, **14**, 131–138.
- 24 B. Ruscic and D. H. Bross, Active Thermochemical Tables (ATcT) values based on ver.1.122d of the Thermochemical-Network, 2018, available at ATcT.anl.gov.
- 25 L. V. Moskaleva and M. C. Lin, *J. Comput. Chem.*, 2000, **21**, 415–425.
- 26 A. Jamal and A. M. Mebel, *Phys. Chem. Chem. Phys.*, 2010, **12**, 2606–2618.
- 27 G. da Silva, *J. Phys. Chem. A*, 2017, **121**, 2086–2095.
- 28 A. J. Colussi, F. Zabel and S. W. Benson, *Int. J. Chem. Kinet.*, 1977, **9**, 161–178.
- 29 C.-Y. Lin and M. C. Lin, *J. Phys. Chem.*, 1986, **90**, 425–431.
- 30 S. Olivella, A. Solé and A. García-Raso, *J. Phys. Chem.*, 1995, **99**, 10549–10556.
- 31 R. Liu, K. Morokuma, A. M. Mebel and M. C. Lin, *J. Phys. Chem.*, 1996, **100**, 9314–9322.
- 32 P. Hemberger, G. D. Silva, A. J. Trevitt, T. Gerber and A. Bodi, *Phys. Chem. Chem. Phys.*, 2015, **17**, 30076–30083.
- 33 M. Shapero, I. A. Ramphal and D. M. Neumark, *J. Phys. Chem. A*, 2018, **122**, 4265–4272.
- 34 D. L. Osborn, H. Choi, D. H. Mordaunt, R. T. Bise, D. M. Neumark and C. M. Rohlfing, *J. Chem. Phys.*, 1997, **106**, 3049–3066.
- 35 A. W. Harrison, M. Ryazanov, E. N. Sullivan and D. M. Neumark, *J. Chem. Phys.*, 2016, **145**, 024305.
- 36 D. Irimia, R. Kortekaas and M. H. M. Janssen, *Phys. Chem. Chem. Phys.*, 2009, **11**, 3958–3966.
- 37 D. Irimia, D. Dobrikov, R. Kortekaas, H. Voet, D. A. van den Ende, W. A. Groen and M. H. M. Janssen, *Rev. Sci. Instrum.*, 2009, **80**, 113303.
- 38 E. Garand, T. I. Yacovitch and D. M. Neumark, *J. Chem. Phys.*, 2009, **130**, 064304.
- 39 J. M. B. Bakker, *J. Phys. E: Sci. Instrum.*, 1973, **6**, 785–789.
- 40 J. M. B. Bakker, *J. Phys. E: Sci. Instrum.*, 1974, **7**, 364–368.
- 41 V. Dribinski, A. Ossadtschi, V. A. Mandelshtam and H. Reisler, *Rev. Sci. Instrum.*, 2002, **73**, 2634–2642.
- 42 O. Jagutzki, A. Cerezo, A. Czasch, R. Dörner, M. Hattas, M. Huang, V. Mergel, U. Spillmann, K. Ullmann-Pfleger, T. Weber, H. Schmidt-Böcking and G. D. W. Smith, *IEEE Trans. Nucl. Sci.*, 2002, **49**, 2477–2483.
- 43 R. A. Marcus and O. K. Rice, *J. Phys. Chem.*, 1951, **55**, 894–908.
- 44 T. Beyer and D. Swinehart, *Commun. ACM*, 1973, **16**, 379.
- 45 M. J. Frisch, G. W. Trucks, H. B. Schlegel, G. E. Scuseria, M. A. Robb, J. R. Cheeseman, G. Scalmani, V. Barone, V. Mennucci, G. A. Petersson, H. Nakatsuji, M. Caricato, X. Li, H. P. Hratchian, A. F. Izmaylov, J. Bloino, G. Zheng, J. L. Sonnenberg, M. Hada, M. Ehara, K. Toyota, R. Fukuda, J. Hasegawa, M. Ishida, T. Nakajima, Y. Honda, O. Kitao, H. Nakai, T. Vreven, J. A. Montgomery, Jr., J. E. Peralta, F. Ogliaro, M. Bearpark, J. J. Heyd, E. Brothers, K. N. Kudin, V. N. Staroverov, T. Keith, R. Kobayashi, J. Normand, K. Raghavachari, A. Rendell, J. C. Burant, S. S. Iyengar, J. Tomasi, M. Cossi, N. Rega, J. M. Millam, M. Klene, J. E. Knox, J. B. Cross, V. Bakken, C. Adamo, J. Jaramillo, R. Gomperts, R. E. Stratmann, O. Yazyev, A. J. Austin, R. Cammi, C. Pomelli, J. W. Ochterski, R. L. Martin, K. Morokuma, V. G. Zakrzewski, G. A. Voth, P. Salvador, J. J. Dannenberg, S. Dapprich, A. D. Daniels, O. Farkas, J. B. Foresman, J. V. Ortiz, J. Cioslowski and D. J. Fox, Gaussian, Inc., Wallingford, CT, 2010.
- 46 M. P. Andersson and P. Uvdal, *J. Phys. Chem. A*, 2005, **109**, 2937–2941.
- 47 V. A. Mozhayskiy and A. I. Krylov, ezSpectrum, <http://iopen.shell.usc.edu/downloads>.
- 48 R. H. Dalitz, *Philos. Mag.*, 1953, **44**, 1068–1080.
- 49 J. Platz, O. J. Nielsen, T. J. Wallington, J. C. Ball, M. D. Hurley, A. M. Straccia, W. F. Schneider and J. Sehested, *J. Phys. Chem. A*, 1998, **102**, 7964–7974.